ACS OMEGA

Open Access

http://pubs.acs.org/journal/acsodf

Article

Gold Nanoparticle-Loaded Silica Nanospheres for Sensitive and Selective Electrochemical Detection of Bisphenol A

Helttoney Antonio Rodrigues da Silva, Keleen M. Barbosa, Raiedhah A. Alsaiari, Gabriela Nunes Silva, João Luiz de Oliveira Maciel Junior, Alex Sander Rodrigues Cangussu, Sergio Bitencourt Araujo Barros, Luelc S. da Costa, José Ribeiro dos Santos Junior, Carla Verônica R. De Moura, Mabkhoot Alsaiari, Vaeudo Valdimiro de Oliveira, Anna K. dos S. Pereira,* Lucas Samuel S. Santos, and Abdur Rahim*

Cite This: *ACS Omega* 2023, 8, 39023−39034

Read Online

ACCESS | Metrics & More | Article Recommendations | Supporting Information

ABSTRACT: In this work, silica nanospheres were used as support for gold nanoparticles and applied for bisphenol A electrochemical detection. The development of new silica-supported materials has attracted increasing attention in the scientific world. One approach of interest is using silica nanospheres as support for gold nanoparticles. These materials have a variety of applications in several areas, such as electrochemical sensors. The obtained materials were characterized by solid-state UV−vis spectroscopy, electron microscopy, X-ray diffraction, and electrochemical techniques. The electrode modified with $AuSiO_2700/CHI/Pt$ was applied as an electrochemical sensor for BPA, presenting an oxidation potential of 0.842 V and a higher peak current among the tested materials. The $AuSiO_2700/CHI/Pt$ electrode showed a logarithmic response for the detection of BPA in the range of 1−1000 nmol L^{-1}, with a calculated detection limit of 7.75 nmol L^{-1} and a quantification limit of 25.8 nmol L^{-1}. Thus, the electrode $AuSiO_2700/CHI/Pt$ was presented as a promising alternative to an electrochemical sensor in the detection of BPA.

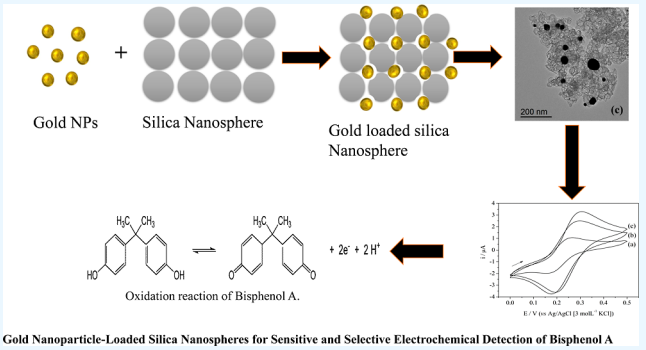

Gold Nanoparticle-Loaded Silica Nanospheres for Sensitive and Selective Electrochemical Detection of Bisphenol A

1. INTRODUCTION

Advances in the development of new materials have provided the use of inorganic solids in the most diverse areas of science. Their applications have undergone a significant expansion, especially when it comes to nanoscale materials since they encompass several applications such as adsorption,[1] wastewater treatment,[2] catalysis,[3] immobilization of biomolecules,[4] drug release,[5,6] encapsulation of molecules,[7] solar cells,[8] and sensors.[9] Especially, the use of nanocomposites and superparamagnetic nanoarchitecture has gained interest for the detection of disease-specific biomarkers.[10] The application of metal nanoparticles-loaded mesoporous silica toward the reduction of organic pollutants was recently reported.[11] Silica nanospheres are structures that may exhibit high monodispersity and surface area.[12] Their stability, chemical versatility, and biocompatibility allow their use in the controlled storage and release of drugs among other applications.[12,13]

Metal nanoparticles exhibit unique physicochemical properties, due to their small size and large specific surface area, as well as optical, electrical, and magnetic properties that differ drastically from the properties of the material on a macroscopic scale. In this way, these nanoparticles can be used as active sites for the transfer of electrons in electrochemical reactions and stand out in the electroanalytical system.[14] Noble metal nanoparticles such as gold are extensively studied. This is because these metals exhibit greater resistance to oxidation and special properties.[15]

A chemical method for the formation of metallic nanoparticles in solid form can be established through the reduction of metallic ions, using metallic precursors in a liquid solution, stabilizing agents, and control of reaction conditions, such as temperature and pH. The method may possibly produce nanoparticles with an adjustable size range.[16]

The use of nanoparticles in the development of new electrochemical sensors and biosensors has allowed us to obtain a better analytical performance. This is because, at the nanoscale, an increase in the active surface area occurs improving the electron transfer, reducing the signal-to-noise ratio, and increasing the response current.[17] Studies using gold nanoparticles were able to demonstrate the simultaneous

Received: May 25, 2023
Accepted: September 15, 2023
Published: October 11, 2023

detection of interfering specimens when analyzed using gold electrodes on a macroscale.[14,18]

Bisphenol A (BPA) is an endocrine-disrupting compound and thus has restricted and prohibited its use in many consumer products.[19,20] Studies involving endocrine disruptors have gained increasing attention.[21] These compounds are initially developed for specific chemicals such as pesticides, plasticizers, or solutions. These substances act as estrogens, and their actions can have side effects when absorbed by the body, potentially altering the animal endocrine system through the inhibition or hormonal blockade, thereby interrupting natural actions and functions.[21] One of the main problems encountered in the determination of these species is related to the complexity of the samples of environmental matrices and in their low concentrations, in the order of ng L^{-1}, although very low, they are physiologically active. This leads to an alert for new studies for the development of methods, mapping tools, and identification of these substances.[20]

With the development of industry, several residual chemicals are being released into the environment. Recently, BPA has attracted great attention due to its estrogenic activity.[22] It is a monomer because it is widely used as an important plasticizer in polymer, epoxy resin, polycarbonate, and other industries. Due to incomplete polymerization processes, BPA monomer residues migrate into food during storage and processing at elevated temperatures or when subjected to sudden cooling,[23] furthermore, this compound is present in products for daily use, such as bottles, electronic equipment, or toys.[24] Due to the large number of BPA applications, human exposure routes are multiple. Studies attribute to this substance problems such as polycystic ovary, female and male fertility problems, abnormal fetal chromosomes, immunological problems and development of reproductive disorders, enlargement of the prostate and urethra, and prostate cancer.[25] Therefore, the health consequences of BPA have been a public concern.

Electrochemical sensors based on nanocomposites, more specifically using gold nanoparticles, have been reported in the literature for BPA detection.[24,26] The big challenge is to achieve low detection capacity, high stability, and reproduction. The combination of silica and gold spheres, both on the nanometer scale, can result in a synergistic effect and, consequently, in a more sensitive and precise electrochemical sensor.

In this sense, the present work aims to develop a nanocomposite of gold nanoparticles deposited in silica nanospheres as a potential electrochemical sensor for BPA.

2. EXPERIMENTAL PART

2.1. Chemical Reagents. Analytical grade chemicals: chloroauric acid ($HAuCl_4$, 99.9%, Sigma-Aldrich), BPA ($C_{15}H_{16}O_2$, 99%, Sigma-Aldrich), acetone (C_3H_6O, 99.5%, Dynamic), acetic acid (CH_3CO_2H, >99.9%, Nuclear), hydrochloric acid (HCl, >37, Vetec), nitric acid (HNO_3, Dynamic), sulfuric acid (H_2SO_4, Vetec), alumina (Al_2O_3, Merk), potassium chloride (KCl, Vetec), commercial ethanol (C_2H_6O, 92.8 INPM, 96 GL), potassium hexacyanoferrate (III) ($K_3[Fe(CN)_6]$, >99, Aldrich), sodium hydroxide (NaOH, Vetec), Pluronic P-123 ($EO_{20}PO_{70}EO_{20}$, Aldrich), chitosan (CHI) [$(C_6H_{11}O_4N)_n$, Polimar], sodium sulfate (Na_2SO_4, Alphatec), tetraethylorthosilicate (TEOS) [$Si(C_2H_5O)_4$, >98, Aldrich], and urea [$(NH_2)_2CO$, Vetec].

2.2. Synthesis of Silica Nanospheres. The silica nanospheres were obtained using a method adopted from a previous study.[27] To this end, 1.0 g Pluronic P123 (M_n = 5800), which is a symmetric triblock copolymer comprising poly(ethylene oxide) (PEO) and poly(propylene oxide) (PPO) in an alternating linear fashion, PEO-PPO-PEO, was added to 30 mL of aqueous HCl solution with pH = 3.88. The mixture was stirred and held at 30 °C until complete dissolution of the polymer. Then, 3.59 mL of silica precursor TEOS was added to this solution under vigorous stirring. After 10 min, the mixture was kept under static conditions at 30 °C for 24 h. The mixture was transferred to an autoclave for hydrothermal treatment in an oven at 100 °C for 24 h. Subsequently, the formed white precipitates were filtered, washed, and oven-dried at 50 °C. The surfactants were removed by refluxing using a 2% HCl solution in ethanol using a Soxhlet extractor. The solids formed were subjected to heat treatment at 550 °C for 6 h at a heating rate of 2 °C min^{-1} in a static air atmosphere.

2.3. Synthesis of Gold Nanoparticles. The procedure described was performed according to ref 28 with modifications in the order of addition of reagents, amount of urea, and concentration of gold precursor. 1.0 g of carrier suspended in 100 mL of deionized water was used. Thereafter, 0.7 g of urea was added and stirred for 5 min. Subsequently, 5 mL of an aqueous solution of $HAuCl_4$ at 12 mmol L^{-1} was added at room temperature under continuous stirring. The mixture was heated to 90 °C and held at this temperature for 4 h under stirring. The solid obtained was separated by centrifugation, washed with 20 mL of deionized water three times, and oven-dried at 50 °C. The material was then separated into two portions, one heated at 300 °C for 6 h and the other portion held at 700 °C for 6 h, both using a heating rate of 10 °C min^{-1} in a quartz tube with synthetic air flow. The resulting materials were named $AuSiO_2300$ and $AuSiO_2700$, according to their temperature in the heat treatment. The follow-up of the synthesis was performed by UV−vis spectroscopy.

2.4. Characterization of Materials. The micrographs of the materials were obtained using secondary and backscattered electrons in a scanning electron microscope FEI Quanta FEG 250 (Thermo) operated at 2 kV. The samples were suspended in isopropanol and sonicated for 15 min, deposited on a brass sample port covered with aluminum foil, and metalized with iridium by a metallizer MED020—Baltic.

Transmission electron microscopy (TEM) measurements were performed at the LME/LNNano/CNPEM in Campinas-SP. A Jeol JEM 2100 HTP electron microscope operated at 200 kV with a LaB_6 electron source was used. The samples, in the form of a fine powder, were suspended using isopropanol ultrasound for 30 min and deposited on ultrafine carbon films.

Solid UV−vis spectra were obtained by using a Shimadzu UV-2450 spectrophotometer and the white precipitate was obtained with barium sulfate (Wako Pure Chemical Industries LTD). The data were obtained in absorbance values.

The UV−vis spectra of $HAuCl_4$ solutions, urea, and the supernatant extracted by centrifugation after the formation reaction of the gold nanoparticles, were obtained by using a T.60 UV−visible spectrophotometer from PG Instruments in the region of 500−600 nm.

X-ray diffractograms were obtained by using a Shimadzu 7000 XRD diffractometer (40 kV, 30 mA) with Cu Kα X-rays (λ = 1.5418 Å), and the diffraction data were recorded at a scan rate of 2.0° min^{-1} with the 2θ angles between 1.4 and 10° for the materials and 5 to 50°. The diameter of the gold

https://doi.org/10.1021/acsomega.3c03607
ACS Omega 2023, 8, 39023−39034

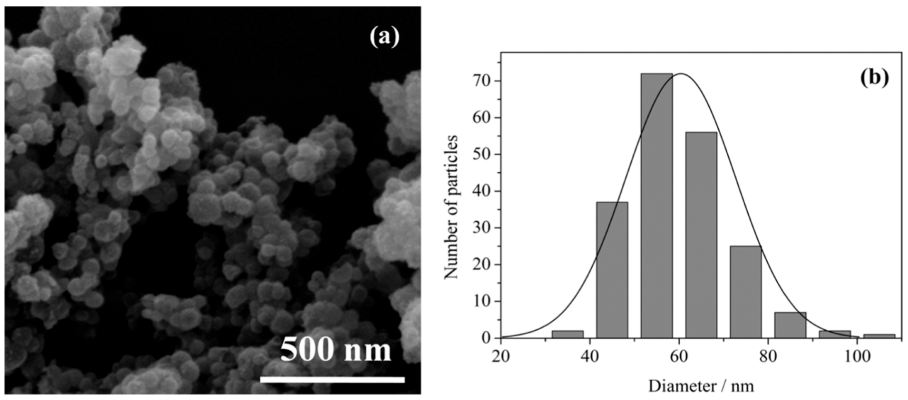

Figure 1. Image obtained by SEM and (b) respective histogram of nanosphere diameters of SiO_2 material

nanoparticles for the materials was calculated using data obtained by XRD and applying the Scherrer equation.

2.5. Electrochemical Characterization. *2.5.1. Preparation of Working Electrodes.* The electrochemical measurements were carried out using a 1 mm-diameter platinum (Pt) electrode, as a working electrode, on which the synthesized materials were deposited. Before the modification, mechanical polishing was carried out on the Pt electrode in a microfiber pad with alumina paste, followed by washing with distilled water until a glass surface was obtained. Then it was placed in 10% H_2SO_4 solution for 10 min. Thereafter, electrochemical cleaning was performed to ensure that the surface was free of interferents and available for the addition of the materials. The obtained materials were placed in 1% CHI solution in the proportion of 1.5 mg of material per 0.5 mL of CHI solution and subjected to an ultrasonic bath to guarantee the stability of the suspension. Then, 3 μL was dripped onto the surface of the working electrode and air-dried.

2.5.2. Electrochemical Measurements and Sensor Evaluation. The electrochemical measurements were performed in a potentiostat/Galvanostat AutoLab Metrohm model PGSTAT302N coupled to a portable computer with software NOVA version 2.1.2. A 0.5 mol L^{-1} solution of Na_2SO_4 was used as a carrier electrolyte. A three-electrode system was used: the working electrode (Pt electrode modified with the materials), a counter electrode (Pt wire), and a Ag/AgCl electrode as the reference electrode.

The electrochemical behavior of the modified electrodes and the determinations of BPA were monitored through cyclic voltammetry (CV) and differential pulse voltammetry (DPV) techniques to evaluate the potential of materials as electrochemical sensors.

3. RESULTS AND DISCUSSION

3.1. Synthesis of Silica Nanospheres. The use of the Pluronic P123 copolymer is essential at this stage, as it is responsible for directing the desired structure; its three-dimensional arrangement favors self-organization.[27] Initially, the polymer was maintained in an acid solution (pH 3.88) and temperature was controlled at 30 °C to obtain structural self-organization. To this solution, was added the silica precursor to form the matrix of interest. Thus, the oxide formed acquires an ordered structure with the polymer filling the pores. The hydrothermal treatment favors the control of pore size and wall thickness. The solids obtained were then subjected to heat treatment to remove the surfactant.[29] The morphology of the material was observed by scanning electron microscopy (SEM), by which it was possible to observe the formation of silica nanospheres, Figure 1a. The material SiO_2 has a structure formed by spheres of similar size. Using SEM images and counting the diameter of more than 100 particles, the histogram of nanosphere diameter distribution was obtained, according to Figure 1b. The mean diameter value of the nanospheres and their respective standard deviation of the SiO_2 measurements was 60.4 (±12.3).

3.2. Synthesis of Gold Nanoparticles. The formation of gold nanoparticles was carried out by per precipitation deposition method using urea. The metal precursor, $HAuCl_4$, was added to an aqueous suspension of the support (SiO_2) and precipitated as hydroxide [hydroxychlorourate (III)]. Synthesis occurred at a controlled temperature of 90 °C, and a change in staining was observed with advancement and reaction time as shown in Figure 2. The complex formed showed a reddish

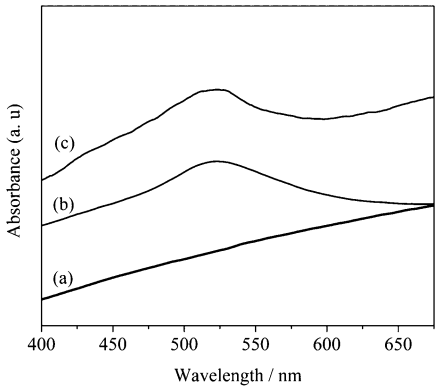

Figure 2. Electronic spectra obtained by diffuse reflectance: (a) SiO_2, (b) $AuSiO_2300$, and (c) $AuSiO_2700$

coloration. This occurs when the anionic hydroxy-chlorate (III) species present in the medium reacts with the positive charge of the surface of the support, generating from this interaction, the nucleation point, providing precipitation of the reddish compound[23,24,30] and is directly related to the amount of Au^{3+} and Au^0 in the solution.

Using the electron spectra obtained from the solution of $HAuCl_4$, urea, and the supernatant extracted by centrifugation after the reaction (Figure S1 from the Supporting Information), it was observed that Au^{3+} was almost completely converted to Au^0, indicating that gold was deposited on the support, which makes this a favorable route in the formation of gold nanoparticles, as described in the literature.[31] Au^{3+} has a

https://doi.org/10.1021/acsomega.3c03607
ACS Omega 2023, 8, 39023−39034

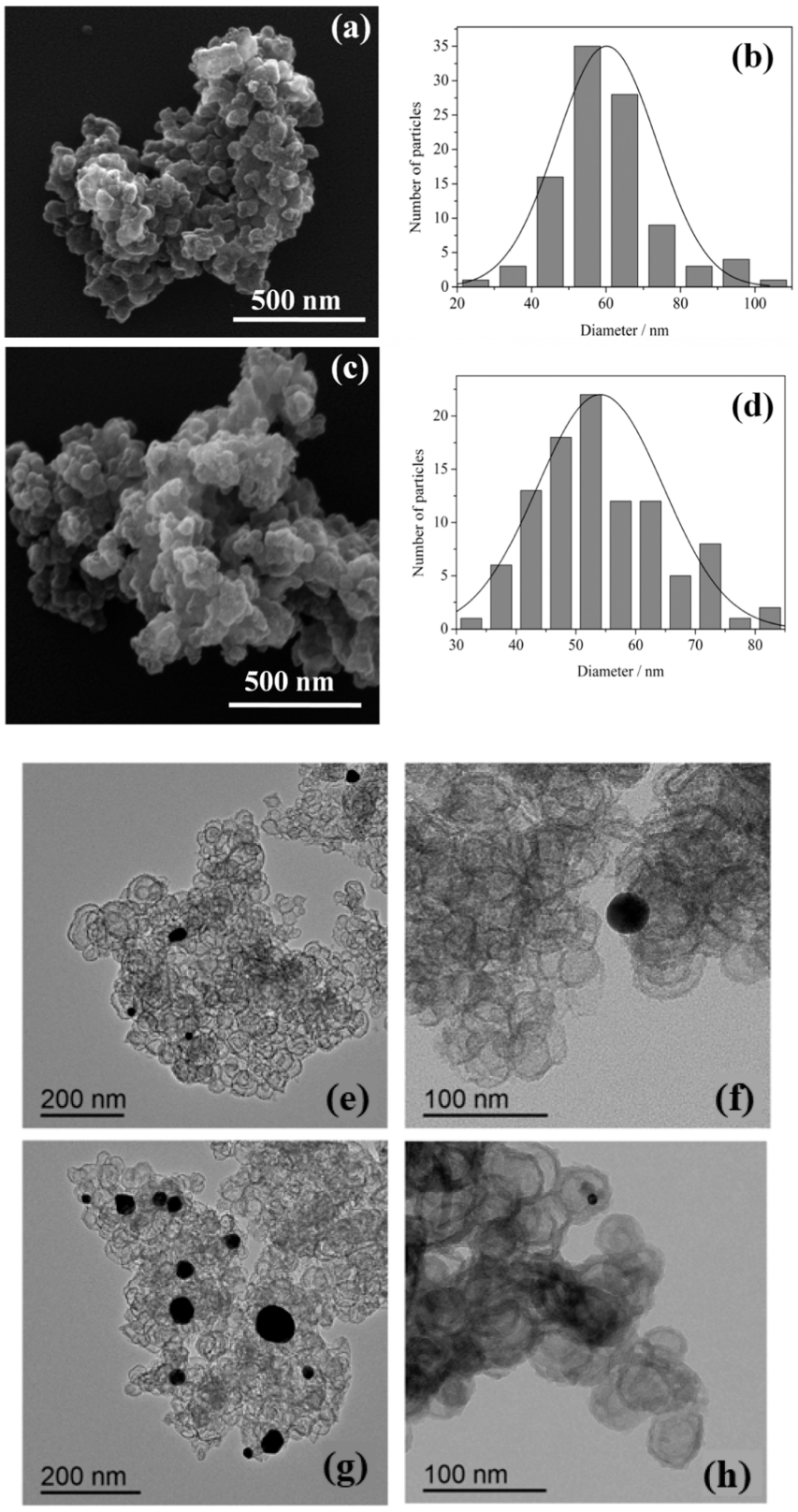

Figure 3. Micrographs obtained by SEM and histograms of the diameters of nanospheres for the material $AuSiO_2300$ (a,b) and for the material $AuSiO_2700$ (c,d). Micrographs were obtained by TEM for the material $AuSiO_2300$ (e,f) and the material $AuSiO_2700$ (g,h)

maximum absorption band at 213 nm. When the absorption spectra of the supernatant and urea were compared, it was observed that the profile of the spectra was similar. This way, it is possible to estimate that the final solution contained only urea, confirming the consumption of Au^{3+} by the disappearance of the absorption band at 213 nm, that is, $Au^{3+} \rightarrow Au^0$. The solid was subjected to thermal treatment at 300 and 700 °C and analyzed by solid-state electronic spectroscopy in the

https://doi.org/10.1021/acsomega.3c03607
ACS Omega 2023, 8, 39023−39034

UV−vis region, which allowed us to observe the formation nature of the nanoparticles.[32] The spectra obtained by diffuse reflectance are shown in Figure 2.

The spectra of the $AuSiO_2300$ and $AuSiO_2700$ materials show maximum absorption bands at 523 and 528 nm, respectively, which characterize the formation of Au nanoparticles of less than 20 nm;[14] a displacement and reduction of the maximum absorption band to 528 nm is still observed, which may be related to the increase of particle size.[33−35] The lengthening and reduction of the intensity of the plasmonic absorption band in the $AuSiO_2700$ material suggests a greater heterogeneity of particle diameter, and the displacement to a greater wavelength characterizes the formation of larger-diameter nanoparticles.[32−34]

The morphology of silica nanospheres decorated with gold nanoparticles could be observed by SEM, according to Figure 3a,c.[29,36] For the materials $AuSiO_2300$ and $AuSiO_2700$, an aggregation of nanospheres occurred, a behavior similar to that observed for SiO_2 material (Figure 1a). This indicates that the nanoparticle synthesis method does not affect the morphology of nanospheres. Histograms of the distribution of the diameters of the nanospheres were constructed, as shown in Figure 3b,d. The average diameters of the nanospheres and their respective standard deviation are 60.1 (±13.4) and 54.1 (±10.6), for the $AuSiO_2300$ and $AuSiO_2700$ materials, respectively (Table 1). For the SiO_2 material, the average diameter of the nanospheres is 60.4 (±12.3). These results show that there are no significant differences in the diameters of the nanospheres. Therefore, it allows us to infer that the methods of forming gold nanoparticles at 300 and 700 °C do not cause an increase in the size of the silica nanospheres (Figure 3a−d).

Table 1. Average Diameter of the Nanospheres of the Materials

material	mean diameter (nm)	number of particles
SiO_2	60.4 (±12.3)	203
$AuSiO_2300$	60.1 (±13.4)	100
$AuSiO_2700$	54.1 (±10.6)	100

TEM micrographs were obtained for the materials after the formation of the gold nanoparticles and are shown in Figure 3e−h. Note that the nanospheres formed were hollow and the Au nanoparticles were dispersed in the materials. A core−shell, with a thin shell, is observed over silica which can be due to the coating of gold shells.[36]

To evaluate the changes in the crystallinity and the mean diameter of the crystallite, X-ray diffraction measurements of the materials containing Au nanoparticles were carried out. According to the pattern described, it is in the range of 5−50° that the first two gold diffraction peaks are observed [Joint Committee on Powder Diffraction Standart (JCPDS) 04-0784]. The materials $AuSiO_2300$ and $AuSiO_2700$ showed peaks at 38.3 and 38.2°, respectively. These peaks correspond to the plane (111) of gold. The second peak observed at 44.5 and 44.4°, respectively, refers to the plane (200) of the cubic face-centered structure (fcc) of gold, as shown in Figure 4.

The materials exhibited characteristic diffraction peaks similar to those of Au. Upon undergoing heat treatment, there was an enhancement in the intensity of the diffraction peaks associated with the crystalline face (111).[35] This is due to the formation of these faces in the nanoparticles.[5,37,38] A

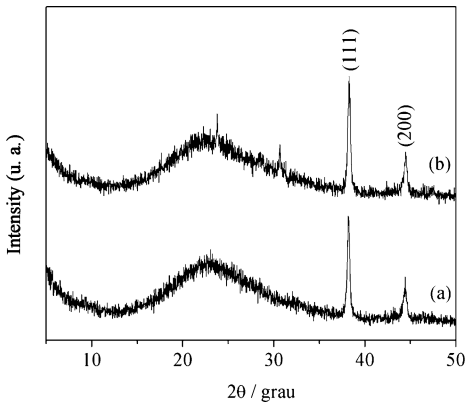

Figure 4. XRD diffractogram of materials: (a) $AuSiO_2300$ and (b) $AuSiO_2700$

large halo appears in the range of 13−31° indicating the presence of noncrystalline SiO_2 in the structure. It can be seen in Figure 3 that the nanoparticles are relatively large and do not present a uniform size, corroborating what the previous study affirms,[32] referring to the per precipitation deposition method using urea to form Au nanoparticles. Thus, the Scherrer equation was used, based on the data obtained in the X-ray diffraction analysis. The mean crystallite size of Au was calculated from the half-height width of the Au (111) diffraction peak (fwhm), using the Scherrer equation (eq 1).[36,39]

$$D = K\lambda/\beta \cos\theta \quad (1)$$

where D is the crystallite diameter, K is proportionality constant, K = 0.9 for spherical particles, λ is the incident wavelength of Cu-kα, 1,5405 Å, β is the half-height width of the peak, and θ is the diffraction angle. The values obtained for the nanoparticles of $AuSiO_2300$ and $AuSiO_2700$, were 25 and 27 nm, respectively (Table 2). As described in the literature,[32,40] when the urea precipitation deposition method is used, the formation of nanoparticles >20 nm occurs. This result is in agreement with that observed by UV−vis spectroscopy and TEM.

Table 2. Particle Size Calculated by the Scherrer Equation

material	fwhm	angle 2θ (degrees)	crystalite diameter (nm)
$AuSiO_2300$	0.33256	38.3	25
$AuSiO_2700$	0.31014	38.2	27

3.3. Electrochemical Study. To evaluate the effect of modifying the surface of the Pt electrode with the materials in the voltammetric response, a study was carried out by the reactions of the redox system of $Fe(CN)_6^{3-/4-}$. The redox reaction of $Fe(CN)_6^{3-/4-}$ is a simple electron transfer process, reversible, and widely explored in the literature for electrode behavior studies.[29,32−34] The electrodes were prepared from the deposition of the two synthesized materials suspended in CHI, resulting in the electrodes $AuSiO_2300$/CHI/Pt and $AuSiO_2700$/CHI/Pt. These were evaluated by CV using a solution of $K_3[Fe(CN)_6]$ 1.0 mmol L^{-1} in Na_2SO_4 0.5 mol L^{-1}. The voltammetry response of the materials was compared with that of the bare Pt electrode. The results are shown in Figure 5.

It can be observed that the electrodes modified with the synthesized materials have a defined redox pair and there is an

https://doi.org/10.1021/acsomega.3c03607
ACS Omega 2023, 8, 39023−39034

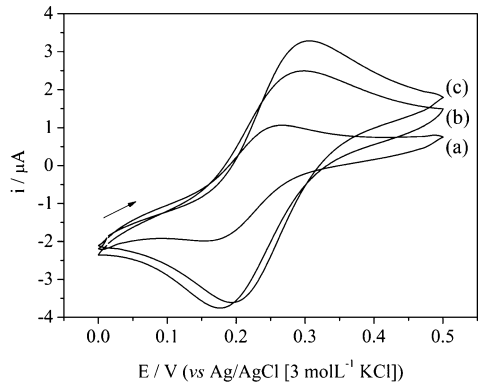

Figure 5. Cyclic voltammograms for the materials: (a) Bare Pt, (b) $AuSiO_2300$/CHI/Pt, and (c) $AuSiO_2700$/CHI/Pt in a solution of $K_3[Fe(CN)_6]$ 1.0 mmol L^{-1} in Na_2SO_4 0.5 mol L^{-1} and υ = 40 mV s^{-1}

increase in the faradaic current when compared to the Pt electrode. The increase in the peak oxidation current from 0.673 μA of the Pt electrode to 1.826 and 2.774 μA when modified with the materials $AuSiO_2300$/CHI/Pt and $AuSiO_2700$/CHI/Pt, respectively, shows that the presence of the materials increases the current intensity, which is related to the increase of the area of the electrode and the process of electron transfer. With the surface modification induced by nanohybrids, there was better sensor performance because it increased the effective surface area and, consequently, increased the probability of capturing an analyte.[41]

The scanning speed ranged from 10 to 70 mV s^{-1}, carried out in a solution of $K_3[Fe(CN)_6]$ 1.0 mmol L^{-1} in Na_2SO_4 0.5 mol L^{-1}. In Figure S2, from the support data, the cyclic voltammograms and respective anode and cathode peak current values as a function of the square root of the scanning speed are presented. It has been found that the relationship between the oxidation peak currents (I_{pa}) and the reduction peak currents (I_{pc}) with the square root of the scanning speed ($\upsilon^{1/2}$) is linear, this dependence shows that the process is controlled by diffusion.[32,33,35,37,42] The effective area of the electrode was obtained through the data extracted from the graphs of $I_{pc} \times \upsilon^{1/2}$ and applied to the Randles−Sevcik equation[43]

$$i_p = (2.69 \times 10^5) n^{3/2} A C D^{1/2} \upsilon^{1/2} \quad (2)$$

in which i_p is the peak current (in A), n is the number of electrons involved in the redox reaction, A is the effective area of the electrode (in cm^2), C is the concentration of the solution of $K_3[Fe(CN)_6]$ (in mmol cm^{-3}), D is the diffusion coefficient of the species [5.49×10^{-8} cm^2 s^{-1} for $K_3[Fe(CN)_6]$ (in cm^2 s^{-1})],[44] and υ is the scanning speed (in V s^{-1}).

The effective area found for the electrodes was 0.0706 cm^2 for the Pt electrode, 0.2818 cm^2 for the electrode $AuSiO_2300$/CHI/Pt, and 0.1074 cm^2 for the electrode $AuSiO_2700$/CHI/Pt; with the modification of the electrode with the materials, there was an increase of the effective area. An increase in area is interesting for electrochemical sensors since it can give rise to a greater number of electroactive sites providing greater sensitivity for the same.[40,45] The presence of the materials offers the electrode a larger effective area.[41,44] The materials $AuSiO_2300$ and $AuSiO_2700$ were subjected to measurements to evaluate their electroanalytical performance. For this, the techniques of CV and DPV were used.

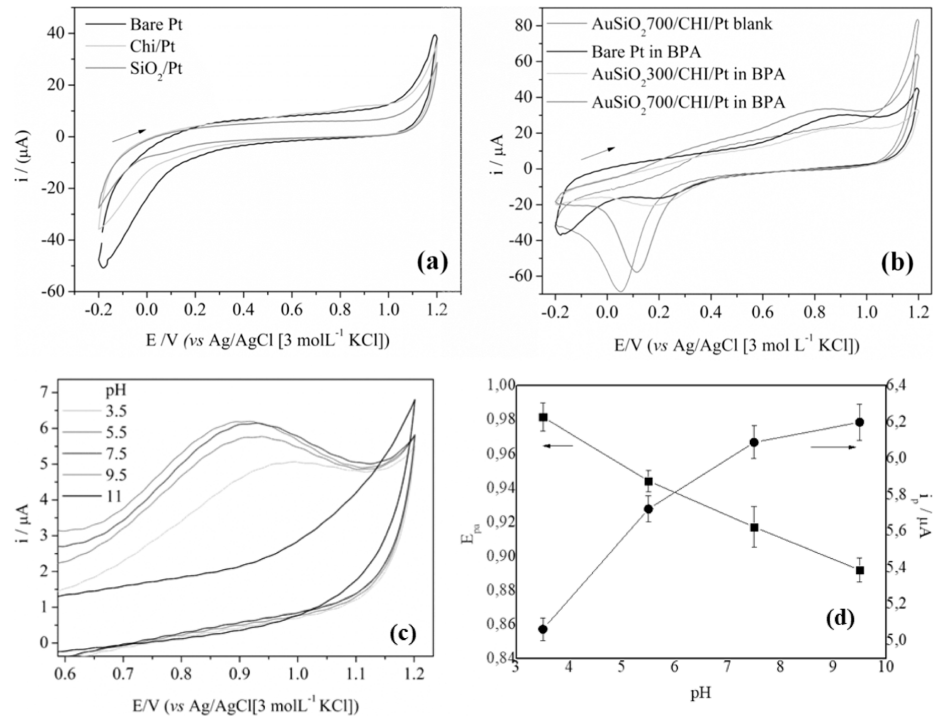

Figure 6. Cyclic voltammograms of the materials in the presence and absence of BPA: In figure (a): (−) blank (0.5 mol L^{-1} of Na_2SO_4), (−) CHI/Pt, and (−) SiO_2/Pt; In figure (b): (−) blank (0.5 mol L^{-1} of Na_2SO_4), (−) bare Pt, (−) $AuSiO_2300$/CHI/Pt, and (−) $AuSiO_2700$/CHI/Pt, in solution of BPA 1×10^{-5} mol L^{-1} (Na_2SO_4 0.5 mol L^{-1}), pH 9.5, and υ = 50 mV. (c) cyclic voltammograms of the electrochemical behavior of BPA 1×10^{-5} mol L^{-1} (Na_2SO_4 0.5 mol L^{-1}) at different pH values: 3.5; 5.5; 7.5; 9.5; and11, υ = 50 mV, and (d) variation of the peaks of current and oxidation potential as a function of pH for the $AuSiO_2700$/CHI/Pt electrode

https://doi.org/10.1021/acsomega.3c03607
ACS Omega 2023, 8, 39023−39034

3.4. Electrochemical Measurements in BPA. The study of the electrochemical behavior of different electrodes in the presence of BPA was investigated by CV. The voltammograms of the materials in the presence of 10 μmol L^{-1} of BPA in Na_2SO_4 0.5 mol L^{-1} (pH 9.5) are shown in Figure 6. Upon conducting tests with various electrolytes, it became evident that the utilization of Na_2SO_4 proved to be more favorable for this system. This choice was attributed to its ability to yield clearer distinctions between oxidation and reduction peaks.

As shown in Figure 6, the silica nanospheres and CHI were not efficient in the oxidation of BPA (Figure 6a). Already the electrodes of Pt, $AuSiO_2$300/CHI/Pt, and $AuSiO_2$700/CHI/Pt presented significant responses for the oxidation of BPA. The electrodes presented peak oxidation potential values of 0.923, 0.898, and 0.842 V for the Pt electrode, $AuSiO_2$300/CHI/Pt, and $AuSiO_2$700/CHI/Pt (Figure 6b), respectively. The cyclic voltammograms presented a single oxidation peak, which indicates that the oxidation reaction of BPA is an irreversible process, such behavior agrees with the other studies described in the literature.[46−50]

A reduction peak is also observed at 0.183, 0.168, and 0.118 V for the Pt electrodes, $AuSiO_2$300/CHI/Pt, and $AuSiO_2$700/CHI/Pt, respectively. These peaks are at the same potential as those described for the reaction of gold-forming gold oxides. According to the literature,[51] electroporation of gold oxides occurs on the surface of the electrodes for solution (reactions 1−3) as described.[52]

These results show that the presence of Au nanoparticles improves the electroanalytical performance of the modified electrode, suggesting that this material may be suitable for the determination of BPA.

The electrode $AuSiO_2$700/CHI/Pt presented the highest oxidation peak current and a lower oxidation potential for BPA, so the other measurements were performed only with this electrode.

The electrochemical behavior of BPA in an aqueous medium was studied by CV in a pH range of 3.5−9.5. The oxidation peak current of BPA is influenced by the pH of the solution as shown in Figure 8. An increase in oxidation peak current and a reduction in oxidation potential with increasing pH in all materials were observed. This behavior is affirmed by the literature.[46,47,53] The BPA has a pK_a of 9.73, that is, its dissociation is favored at very alkaline pH (Figure 6c). Thus, the undissociated BPA can be better absorbed than the dissociated BPA.[49]

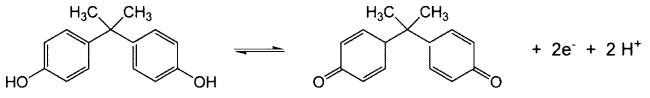

Figure 7. Oxidation reaction of BPA

Considering that the increase in pH shifts the reaction toward the oxidation of BPA since H^+ consumption occurs,[53] the pH of the medium was defined as 9.5 in an attempt to obtain a better performance of the electrode as a sensor. The relationship between the oxidation potential (E_{pa}) and pH was also shown in Figure 6b, and a linear displacement of E_{pa} toward the negative potential with increasing pH indicated that the protons were directly involved in the oxidation of BPA (Figures 7and 8). This indicates that the number of electrons transferred in the electrode reaction is accompanied by an equal number of protons. Therefore, as pH increases, there is a consumption of H^+ ions, causing the reaction to shift in the direction of BPA oxidation.[47]

Figure 8 shows the relationship between the oxidation peak current ($i_{pa}/\mu A$) and the square root of the scanning rate [$\upsilon^{1/2}/(mV\ s^{-1})$], where it is observed that with increasing scanning, there is an increase in the peak current and a small displacement of the potential of the peak of oxidation to a more positive potential, which is a characteristic behavior of irreversible processes.[49]

Note that the peak current increased linearly with the square root of the scanning velocity in the range of 10−70 mV s^{-1} and can be expressed by eq 3

$$i_{pa}/(\mu A) = -0.1704(\pm 0.0251) + 3.0814(\pm 0.1257)\upsilon^{1/2}/(mVs^{-1}),\quad R^2 = 0.9901 \tag{3}$$

This indicates that the oxidation of BPA on the $AuSiO_2$700/CHI/Pt electrode is a diffusion-controlled process.[54] With increasing scanning velocity, E_{pa} varied positively in a linear relationship, so the relationship between the potential of anode peak (E_{pa}) and the natural logarithm of the scanning velocity (ln υ) was obtained and can be expressed by eq 4

$$E_{pa}/(V) = 1.1164(\pm 0.0241) + 0.0596(\pm 0.0070)\ln \upsilon,\ R^2 = 0.9227 \tag{4}$$

For a fully irreversible electrode process, the relationship between E_{pa} and ln υ is expressed by the Lairon equation[48,54]

$$\text{pen}^0 + \left(\frac{RT}{\alpha nF}\right)\ln\left(\frac{RTk^\circ}{\alpha nF}\right) + \left(\frac{RT}{\alpha nF}\right)\ln \upsilon \tag{5}$$

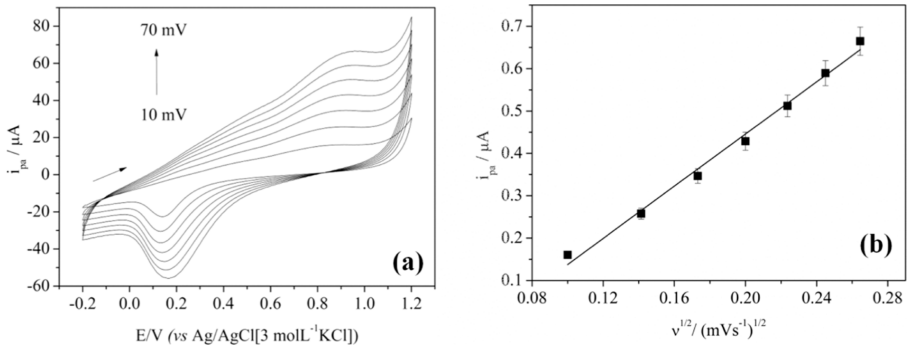

Figure 8. Cyclic voltammograms with scanning speed variation for the electrode $AuSiO_2$700/CHI/Pt: (a) CV of the scanning speed and (b) graph of i_{pa} as a function of $\upsilon^{1/2}$, in the presence of BPA 1 × 10^{-5} mol L^{-1} (Na_2SO_4 0.5 mol L^{-1}), pH 9.5

https://doi.org/10.1021/acsomega.3c03607
ACS Omega 2023, 8, 39023−39034

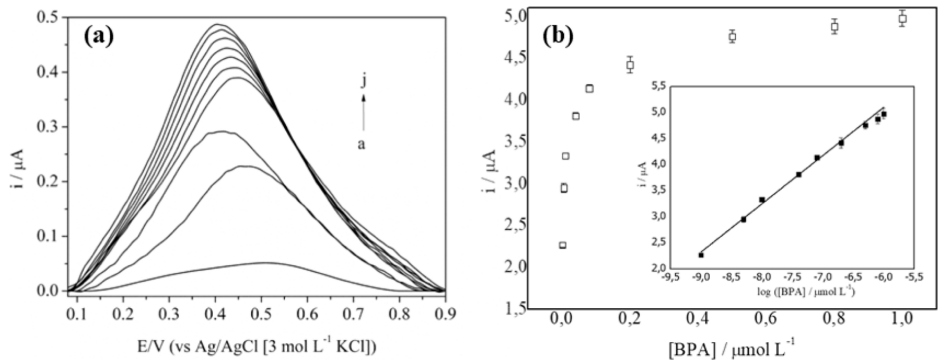

Figure 9. (a) Differential pulse voltammogram at different concentrations of BPA for the electrode $AuSiO_2700/CHI/Pt$: (i) white precipitate (Na_2SO_4 0.5 mol L^{-1} as an electrolyte support and pH = 9.5); it was determined by measuring replicates of a blank sample and calculated using the mean result and standard deviation (n = 3), (ii) 0.001; (iii) 0.005; (iv) 0.010; (v) 0.040; (vi) 0.080; (vii) 0.200; (viii) 0.500; (ix) 0.800, and (x) 1.000 μmol L^{-1} in Na_2SO_4 0.5 mol L^{-1} as electrolyte support and pH = 9.5 and (b) Analytical curve for BPA

Table 3. Comparison between the Parameters of the Proposed Sensor and Other Electroanalytical Methods Described in the Literature for the Detection of BPA

sensor	linear region	LOD	technique	reference
$AuSiO_2700/CHI/Pt$	0.001−1 μmol L^{-1}	7.75 nmol L^{-1}	DPV	this article
AuPdNPs/GNs	0.05−10 μmol L^{-1}	8.0 nmol L^{-1}	DPV	49
CS/N-GS/GCE	0.01−1.30 μmol L^{-1}	5.0 nmol L^{-1}	AMP	46
LDH/GCE	0.01−1.05 μmol L^{-1}	5.0 nmol L^{-1}	DPV	56
Pt/PDDA-DMP/GCE	5.00−30.0 μmol L^{-1}	600 nmol L^{-1}	DPV	51
Grafeno/GCE	0.05−1.00 μmol L^{-1}	47 nmol L^{-1}	DPV	47
Cu_2O-rGO	0.10−80.0 μmol L^{-1}	53 nmol L^{-1}	CV	48
SBA-MIP	0.10−500 μmol L^{-1}	32 nmol L^{-1}	CV	57
ELDH/GCE	0.02−1.51 μmol L^{-1}	6.8 nmol L^{-1}	DPV	54

where: α is the electron transfer coefficient, k^0 is the standard rate constant of the reaction, n is the electron transfer number involved in the redox reaction, υ is the scanning speed, and E^0 is the formal potential. The other symbols have their usual meanings. Thus, the value αn be calculated from the slope of E_{pa}−ln υ. For the proposed electrode, the slope is 0.0596 (±0.0070), so the value of αn was calculated as being 0.991 (taking T = 298 K, R = 8.314 J mol^{-1} K^{-1}, and F = 96,480 C). According to the literature, α is defined as 0.5 in the irreversible electrode process.[54] Thus, the number of electrons (n) transferred in the oxidation of BPA is 1.982, approximately 2. Based on the result obtained in the relation between the E_{pa} and pH, in which the number of electrons and protons involved in the BPA oxidation process is equal, the oxidation of BPA on the surface of the $AuSiO_2700/CHI/Pt$ electrode is a process involving the transfer of two electrons and two protons.

3.5. Analytical Performance. The analytical performance of the $AuSiO_2700/CHI/Pt$ electrode as a sensor in the detection of BPA was studied using DPV. Figure 9a shows the voltammograms of DPV for the different concentrations of the analyte. The results show that the intensity of the current increased in logarithmic proportions with the increase of BPA concentration in the range of 1.0−1000 nmol L^{-1}. The analytical curve of current vs logarithm of BPA concentration (mol L^{-1}) was constructed in Figure 9b.

For this concentration range, we obtained an analytical curve with good linearity (R^2 = 0.995) and sensitivity of 0.8911 (±0.0224).log (C_{BPA}/ mol L^{-1}). The linear regression equation can be expressed by

$$i_p/(\mu A) = 10.374(\pm 0.1631) + 0.8911(\pm 0.0224)\cdot\log(C_{BPA}/\text{mol L}^{-1}) \quad R^2 = 0.995 \quad (6)$$

To determine the limits of detection (LOD) and quantification (LOQ) for the method, we utilized the analytical curve data.[53] The values of LOD and LOQ were estimated at 7.75 nmol L^{-1} and 2.58 × 10^{-8} mol L^{-1}, respectively.

In Table 3 it is possible to compare the values obtained with the proposed sensor $AuSiO_2700/CHI/Pt$ against other materials described in the literature. The $AuSiO_2700/CHI/Pt$ presented a detection limit in the same order of magnitude as the materials with lower LOD values. In addition, the material presented a wide measurement range among the materials described, which makes this material interesting when it is desired to work with great variations in the concentrations of the analyte of interest. Although $AuSiO_2700/CHI/Pt$ has a less wide linear range than some other sensors, its performance was close to that of most of them and with satisfactory detection results. The calculated LOD is 7.75 nmol L^{-1}, and the electrode used showed a linear response from 1.0 nmol L^{-1}.

The success of nanocomposites is noticeable. In this sense, the Au plasmonic and silica dielectric configurations have been used for smart biosensor technologies. With these nanocomposites, Bhaskar et al. reported an LOD for spermidine in the order of femtomolar,[55] and Rai et al.[56] reported the detection of rhodamine B in the femtomolar order. The method applied by the authors allows a multitude of detection and diagnostic applications and detection of substances in low concentration.[57]

3.6. Selectivity, Reproducibility, and Stability. The selectivity and specificity of the proposed sensor were assessed

https://doi.org/10.1021/acsomega.3c03607
ACS Omega 2023, 8, 39023−39034

in the presence of coexisting species such as catechol, resorcinol, hydroquinone, and nitrite. To verify the selectivity, double concentrations (0.20 μmol L^{-1}) of the interfering species were introduced, yet no discernible response was observed in the proposed sensor's output. This observation solidifies the notion that the proposed sensor exhibits selectivity for BPA determination, as depicted in Figure S4.

Moreover, the reproducibility and stability of the electrode fabrication were gauged by preparing five distinct electrodes. Their current responses were analyzed in the presence of 0.080 μmol L^{-1} of BPA. Notably, the electrodes exhibited consistent current responses, with minimal variation and a relative standard deviation of ±0.0013. This outcome affirms that variations in sensor fabrication methods do not influence the electrochemical response. The effective working area of the electrode remained consistent across different electrodes, as demonstrated in Table S1.

4. CONCLUSIONS

The silica nanospheres were successfully synthesized and confirmed in SEM micrographs. It was possible to observe their well-defined morphology and the formation of nanosphere aggregates. The gold nanoparticles ($AuSiO_2300$ and $AuSiO_2700$) were synthesized by the precipitation deposition method using urea and $HAuCl_4$ as a gold precursor. Heat treatment was a decisive step in the formation of nanoparticles. The characterization of these materials was performed by SEM, TEM, UV−vis spectroscopy, and XRD. It was possible to observe that the calcination temperature favors the aggregation of the particles, which favors an increase in the size of the nanoparticles. The materials $AuSiO_2300$ and $AuSiO_2700$ presented electrocatalytic activity for the oxidation of BPA. After electrode modification, the performance remarkably improved. $AuSiO_2700$/CHI/Pt was the one that presented the best performance among the electrodes tested, with a higher peak current value and a lower peak oxidation potential. The electrode modified with $AuSiO_2700$/CHI/Pt exhibited a linear response for the detection of BPA in the range of 1.0−1000 nmol L^{-1}, with an LOD of 7.75 nmol L^{-1} and an LOQ of 2.58×10^{-8} mol L^{-1}. These values are in the same order of magnitude as the other materials described in the literature and have a wide range of concentrations, showing that the material has application potential as a BPA sensor. Therefore, a new electrochemical method, simple and efficient, was successfully proposed for the determination of BPA.[58]

■ ASSOCIATED CONTENT

Supporting Information

The Supporting Information is available free of charge at https://pubs.acs.org/doi/10.1021/acsomega.3c03607.

Different stages of the gold nanoparticle formation reaction, UV−vis spectra of the $HAuCl_4$ solution at different times and 23.3 mmol L^{-1} urea solution, cyclic voltammograms obtained at scan rates for all electrodes, selectivity study, and current response of different electrodes (PDF)

■ AUTHOR INFORMATION

Corresponding Authors

Anna K. dos S. Pereira − *Universidade Federal do Tocantins, Campus de Gurupi, Gurupi 77001-090 Tocantins, Brazil*; Email: anna_karla@uft.edu.br

Abdur Rahim − *Department of Chemistry, COMSATS University, Islamabad 45550, Pakistan*; orcid.org/0000-0002-2102-658X; Email: rahimkhan533@gmail.com

Authors

Helttoney Antonio Rodrigues da Silva − *Universidade Federal do Tocantins, Campus de Gurupi, Gurupi 77001-090 Tocantins, Brazil*

Keleen M. Barbosa − *Universidade Federal do Tocantins, Campus de Gurupi, Gurupi 77001-090 Tocantins, Brazil*

Raiedhah A. Alsaiari − *Department of Chemistry, Faculty of Science and Arts at Sharurah, Najran University, Sharurah 68342, Saudi Arabia*

Gabriela Nunes Silva − *Universidade Federal do Tocantins, Campus de Gurupi, Gurupi 77001-090 Tocantins, Brazil*

João Luiz de Oliveira Maciel Junior − *Universidade Federal do Tocantins, Campus de Gurupi, Gurupi 77001-090 Tocantins, Brazil*

Alex Sander Rodrigues Cangussu − *Universidade Federal do Tocantins, Campus de Gurupi, Gurupi 77001-090 Tocantins, Brazil*

Sergio Bitencourt Araujo Barros − *Universidade Estadual do Piauí, Picos 64002-150 Piauí, Brazil*

Luelc S. da Costa − *National Nanotechnology Laboratory (LNNano), National Center for Research in Energy and Materials (CNPEM), Campinas CEP: 13083-970 São Paulo, Brazil*

José Ribeiro dos Santos Junior − *Federal University of Piauí, Teresina 64049-550 Piauí, Brazil*

Carla Verônica R. De Moura − *Federal University of Piauí, Teresina 64049-550 Piauí, Brazil*; orcid.org/0000-0003-0998-5929

Mabkhoot Alsaiari − *Department of Chemistry, Faculty of Science and Arts at Sharurah, Najran University, Sharurah 68342, Saudi Arabia*

Vaeudo Valdimiro de Oliveira − *Federal University of Piauí, Teresina 64049-550 Piauí, Brazil*

Lucas Samuel S. Santos − *Universidade Federal do Tocantins, Campus de Gurupi, Gurupi 77001-090 Tocantins, Brazil*

Complete contact information is available at: https://pubs.acs.org/10.1021/acsomega.3c03607

Notes

The authors declare no competing financial interest.

■ ACKNOWLEDGMENTS

We thank CAPES for the scholarship to H.A.R.d.S. and A.K.d.S.P. We also thank the CNPEM LNNano for the analysis of TEM and Unicamp for the analysis of electron spectroscopy in the visible ultraviolet region and X-ray diffraction and to the UFPI for the analysis of SEM and electrochemical characterization. The authors would like to acknowledge the support of the Deputy for Research and Innovation Ministry of Education, Kingdom of Saudi Arabia, for this research through a grant (NU/RG/SERC/12/1) under the Institutional Funding Committee at Najran University, Kingdom of Saudi Arabia.

■ REFERENCES

(1) Vathyam, R.; Wondimu, E.; Das, S.; Zhang, C.; Hayes, S.; Tao, Z.; Asefa, T. Improving the adsorption and release capacity of organic-functionalized mesoporous materials to drug molecules with temper-

https://doi.org/10.1021/acsomega.3c03607
ACS Omega 2023, 8, 39023−39034

ature and synthetic methods. *J. Phys. Chem. C* **2011**, *115* (27), 13135−13150.
(2) Iqbal, J.; Shah, N. S.; Khan, Z. U. H.; Rizwan, M.; Murtaza, B.; Jamil, F.; Shah, A.; Ullah, A.; Nazzal, Y.; Howari, F. Visible light driven doped CeO2 for the treatment of pharmaceuticals in wastewater: A review. *J. Water Proc. Eng.* **2022**, *49*, 103130.
(3) (a) Gutiérrez, L. F.; Hamoudi, S.; Belkacemi, K. Synthesis of gold catalysts supported on mesoporous silica materials: recent developments. *Catalysts* **2011**, *1* (1), 97−154. (b) Li, H.; Wang, R.; Hong, Q.; Chen, L.; Zhong, Z.; Koltypin, Y.; Calderon-Moreno, J.; Gedanken, A. Ultrasound-assisted polyol method for the preparation of SBA-15-supported ruthenium nanoparticles and the study of their catalytic activity on the partial oxidation of methane. *Langmuir* **2004**, *20* (19), 8352−8356. (c) Sunil Sekhar, A. C.; Vinod, C. P. Gold incorporated mesoporous silica thin film model surface as a robust SERS and catalytically active substrate. *Molecules* **2016**, *21* (5), 667. (d) Wu, H.; Pantaleo, G.; Venezia, A. M.; Liotta, L. F. Mesoporous silica based gold catalysts: Novel synthesis and application in catalytic oxidation of CO and volatile organic compounds (VOCs). *Catalysts* **2013**, *3* (4), 774−793.
(4) Itoh, T.; Hoshikawa, Y.; Matsuura, S.-i.; Mizuguchi, J.; Arafune, H.; Hanaoka, T.-a.; Mizukami, F.; Hayashi, A.; Nishihara, H.; Kyotani, T. Production of L-theanine using glutaminase encapsulated in carbon-coated mesoporous silica with high pH stability. *Biochem. Eng. J.* **2012**, *68*, 207−214.
(5) Hu, Y.; Xu, M.; Liu, Y.; Xie, X.; Bao, W.; Song, A.; Hao, J. CHI gel incorporated peptide-modified AuNPs for sustained drug delivery with smart pH responsiveness. *J. Mater. Chem. B* **2017**, *5* (6), 1174−1181.
(6) Wang, Y.; Zhao, Q.; Han, N.; Bai, L.; Li, J.; Liu, J.; Che, E.; Hu, L.; Zhang, Q.; Jiang, T.; et al. Mesoporous silica nanoparticles in drug delivery and biomedical applications. *Nanomed. Nanotechnol. Biol. Med.* **2015**, *11* (2), 313−327.
(7) (a) Janatova, A.; Bernardos, A.; Smid, J.; Frankova, A.; Lhotka, M.; Kourimská, L.; Pulkrabek, J.; Kloucek, P. Long-term antifungal activity of volatile essential oil components released from mesoporous silica materials. *Ind. Crops Prod.* **2015**, *67*, 216−220. (b) Ribes, S.; Ruiz-Rico, M.; Pérez-Esteve, É.; Fuentes, A.; Talens, P.; Martínez-Máñez, R.; Barat, J. M. Eugenol and thymol immobilised on mesoporous silica-based material as an innovative antifungal system: Application in strawberry jam. *Food Control* **2017**, *81*, 181−188. (c) Ruiz-Rico, M.; Daubenschüz, H.; Perez-Esteve, E.; Marcos, M. D.; Amoros, P.; Martinez-Manez, R.; Barat, J. M. Protective effect of mesoporous silica particles on encapsulated folates. *Eur. J. Pharm. Biopharm.* **2016**, *105*, 9−17.
(8) (a) Lee, K.; Yoon, C.-M.; Noh, J.; Jang, J. Morphology-controlled mesoporous SiO 2 nanorods for efficient scaffolds in organo-metal halide perovskite solar cells. *Chem. Commun.* **2016**, *52* (22), 4231−4234. (b) Zhang, Y.; Zhang, Z.; Yan, W.; Zhang, B.; Feng, Y.; Asiri, A. M.; Nazeeruddin, M. K.; Gao, P. Hexagonal mesoporous silica islands to enhance photovoltaic performance of planar junction perovskite solar cells. *J. Mater. Chem. A* **2017**, *5* (4), 1415−1420. (c) Zhao, T.; Luo, W.; Deng, Y.; Luo, Y.; Xu, P.; Liu, Y.; Wang, L.; Ren, Y.; Jiang, W. Monodisperse mesoporous TiO2 microspheres for dye sensitized solar cells. *Nano Energy* **2016**, *26*, 16−25.
(9) Hou, C.; Tang, W.; Zhang, C.; Wang, Y.; Zhu, N. A novel and sensitive electrochemical sensor for bisphenol A determination based on carbon black supporting ferroferric oxide nanoparticles. *Electrochim. Acta* **2014**, *144*, 324−331.
(10) (a) Haq Khan, Z. U.; Khan, T. M.; Khan, A.; Shah, N. S.; Muhammad, N.; Tahir, K.; Iqbal, J.; Rahim, A.; Khasim, S.; Ahmad, I.; et al. Brief review: Applications of nanocomposite in electrochemical sensor and drugs delivery. *Front. Chem.* **2023**, *11*, 1152217. (b) Masud, M. K.; Na, J.; Younus, M.; Hossain, M. S. A.; Bando, Y.; Shiddiky, M. J.; Yamauchi, Y. Superparamagnetic nanoarchitectures for disease-specific biomarker detection. *Chem. Soc. Rev.* **2019**, *48* (24), 5717−5751. (c) Bakshi, S.; Mehta, S.; Kumeria, T.; Shiddiky, M. J.; Popat, A.; Choudhury, S.; Bose, S.; Nayak, R. Rapid fabrication of homogeneously distributed hyper-branched gold nanostructured electrode based electrochemical immunosensor for detection of protein biomarkers. *Sens. Actuators, B* **2021**, *326*, 128803.
(11) Habeche, F.; Boukoussa, B.; Issam, I.; Mokhtar, A.; Lu, X.; Iqbal, J.; Benali, F.; Hacini, S.; Hachemaoui, M.; Abboud, M. Synthesis and application of metal nanoparticles-loaded mesoporous silica toward the reduction of organic pollutants in a simple and binary system. *Inorg. Chem. Commun.* **2023**, *151*, 110572.
(12) Slowing, I. I.; Vivero-Escoto, J. L.; Wu, C.-W.; Lin, V. S.-Y. Mesoporous silica nanoparticles as controlled release drug delivery and gene transfection carriers☆. *Adv. Drug Deliv. Rev.* **2008**, *60* (11), 1278−1288.
(13) (a) Bharathi, S.; Nogami, M.; Ikeda, S. Novel electrochemical interfaces with a tunable kinetic barrier by self-assembling organically modified silica gel and gold nanoparticles. *Langmuir* **2001**, *17* (1), 1−4. (b) Mekaru, H.; Lu, J.; Tamanoi, F. Development of mesoporous silica-based nanoparticles with controlled release capability for cancer therapy. *Adv. Drug Deliv. Rev.* **2015**, *95*, 40−49.
(14) de Menezes, E. W.; Nunes, M. R.; Arenas, L. T.; Dias, S. L.; Garcia, I. T.; Gushikem, Y.; Costa, T. M.; Benvenutti, E. V. Gold nanoparticle/charged silsesquioxane films immobilized onto Al/SiO 2 surface applied on the electrooxidation of nitrite. *J. Solid State Electrochem.* **2012**, *16*, 3703−3713.
(15) Marakatti, V. S.; Peter, S. C. Nickel−antimony nanoparticles confined in SBA-15 as highly efficient catalysts for the hydrogenation of nitroarenes. *New J. Chem.* **2016**, *40* (6), 5448−5457.
(16) Ahmad, T.; Iqbal, J.; Bustam, M. A.; Irfan, M.; Anwaar Asghar, H. M. A critical review on phytosynthesis of gold nanoparticles: Issues, challenges and future perspectives. *J. Clean. Prod.* **2021**, *309*, 127460.
(17) (a) Cao, H.; He, J.; Deng, L.; Gao, X. Fabrication of cyclodextrin-functionalized superparamagnetic Fe3O4/amino-silane core−shell nanoparticles via layer-by-layer method. *Appl. Surf. Sci.* **2009**, *255* (18), 7974−7980. (b) Gupta, R.; Rastogi, P. K.; Ganesan, V.; Yadav, D. K.; Sonkar, P. K. Gold nanoparticles decorated mesoporous silica microspheres: a proficient electrochemical sensing scaffold for hydrazine and nitrobenzene. *Sens. Actuators, B* **2017**, *239*, 970−978.
(18) (a) de Lima, C. A.; Santana, E. R.; Piovesan, J. V.; Spinelli, A. Silver nanoparticle-modified electrode for the determination of nitro compound-containing pesticides. *Anal. Bioanal. Chem.* **2016**, *408*, 2595−2606. (b) Ragavan, K.; Rastogi, N. K.; Thakur, M. Sensors and biosensors for analysis of bisphenol-A. *TrAC, Trends Anal. Chem.* **2013**, *52*, 248−260.
(19) Czarny-Krzymińska, K.; Krawczyk, B.; Szczukocki, D. Bisphenol A and its substitutes in the aquatic environment: Occurrence and toxicity assessment. *Chemosphere* **2023**, *315*, 137763.
(20) Rahman, M. A.; Shiddiky, M. J.; Park, J.-S.; Shim, Y.-B. An impedimetric immunosensor for the label-free detection of bisphenol A. *Biosens. Bioelectron.* **2007**, *22* (11), 2464−2470.
(21) (a) Caserta, D.; Maranghi, L.; Mantovani, A.; Marci, R.; Maranghi, F.; Moscarini, M. Impact of endocrine disruptor chemicals in gynaecology. *Hum. Reprod. Update* **2007**, *14* (1), 59−72. (b) Schug, T. T.; Janesick, A.; Blumberg, B.; Heindel, J. J. Endocrine disrupting chemicals and disease susceptibility. *J. Steroid Biochem. Mol. Biol.* **2011**, *127* (3−5), 204−215.
(22) Anvisa, P. Disponível em. http://portal.anvisa.gov.br (accessesd 07 28, 2019). (b) Bernardo, P. E. M.; Navas, S. A.; Murata, L. T. F.; Alcântara, M. R. d. S. d. Bisphenol A: review on its use in the food packaging, exposure and toxicity. *R. Inst. Adolfo Lutz* **2015**, *74*, 1−11.
(23) Geens, T.; Aerts, D.; Berthot, C.; Bourguignon, J.-P.; Goeyens, L.; Lecomte, P.; Maghuin-Rogister, G.; Pironnet, A.-M.; Pussemier, L.; Scippo, M.-L.; et al. A review of dietary and non-dietary exposure to bisphenol-A. *Food Chem. Toxicol.* **2012**, *50* (10), 3725−3740.
(24) Nodehi, M.; Baghayeri, M.; Behazin, R.; Veisi, H. Electrochemical aptasensor of bisphenol A constructed based on 3D mesoporous structural SBA-15-Met with a thin layer of gold nanoparticles. *Microchem. J.* **2021**, *162*, 105825.

https://doi.org/10.1021/acsomega.3c03607
ACS Omega 2023, 8, 39023−39034

(25) Teeguarden, J. G.; Hanson-Drury, S. A systematic review of Bisphenol A "low dose" studies in the context of human exposure: A case for establishing standards for reporting "low-dose" effects of chemicals. *Food Chem. Toxicol.* **2013**, *62*, 935−948.
(26) (a) Baumgarten, L. G.; Freitas, A. A.; Santana, E. R.; Winiarski, J. P.; Dreyer, J. P.; Vieira, I. C. Graphene and gold nanoparticle-based bionanocomposite for the voltammetric determination of bisphenol A in (micro) plastics. *Chemosphere* **2023**, *334*, 139016. (b) Zhang, X.; Zhu, J.; Wu, Z.; Wen, W.; Zhang, X.; Wang, S. Electrochemical sensor based on confined synthesis of gold nanoparticles@ covalent organic frameworks for the detection of bisphenol A. *Anal. Chim. Acta* **2023**, *1239*, 340743.
(27) Yang, Y.; Karmakar, S.; Zhang, J.; Yu, M.; Mitter, N.; Yu, C. Synthesis of SBA-15 rods with small sizes for enhanced cellular uptake. *J. Mater. Chem. B* **2014**, *2* (30), 4929−4934.
(28) Gualteros, J. A.; Garcia, M. A.; da Silva, A. G.; Rodrigues, T. S.; Cândido, E. G.; e Silva, F. A.; Fonseca, F. C.; Quiroz, J.; de Oliveira, D. C.; de Torresi, S. I. C.; et al. Synthesis of highly dispersed gold nanoparticles on Al 2 O 3, SiO 2, and TiO 2 for the solvent-free oxidation of benzyl alcohol under low metal loadings. *J. Mater. Sci.* **2019**, *54*, 238−251.
(29) Xu, S.; Hartvickson, S.; Zhao, J. X. Increasing surface area of silica nanoparticles with a rough surface. *ACS Appl. Mater. Interfaces* **2011**, *3* (6), 1865−1872.
(30) Diamanti-Kandarakis, E.; Bourguignon, J.-P.; Giudice, L. C.; Hauser, R.; Prins, G. S.; Soto, A. M.; Zoeller, R. T.; Gore, A. C. Endocrine-disrupting chemicals: an Endocrine Society scientific statement. *Endocr. Rev.* **2009**, *30* (4), 293−342.
(31) (a) Wang, L.-C.; Liu, Q.; Huang, X.-S.; Liu, Y.-M.; Cao, Y.; Fan, K.-N. Gold nanoparticles supported on manganese oxides for low-temperature CO oxidation. *Appl. Catal. B Environ.* **2009**, *88* (1−2), 204−212. (b) Zanella, R.; Giorgio, S.; Henry, C. R.; Louis, C. Alternative methods for the preparation of gold nanoparticles supported on TiO2. *J. Phys. Chem. B* **2002**, *106* (31), 7634−7642.
(32) Oliveira, R. L.; Zanchet, D.; Kiyohara, P. K.; Rossi, L. M. On the Stabilization of Gold Nanoparticles over Silica-Based Magnetic Supports Modified with Organosilanes. *Chem.−Eur. J.* **2011**, *17* (16), 4626−4631.
(33) Fattori, N.; Maroneze, C. M.; da Costa, L. P.; Strauss, M.; Sigoli, F. A.; Mazali, I. O.; Gushikem, Y. Ion-exchange properties of Imidazolium-grafted SBA-15 toward AuCl4−anions and their conversion into supported gold nanoparticles. *Langmuir* **2012**, *28* (27), 10281−10288.
(34) Melo Jr, M. A., Jr.; Santos, L. S. S.; Gonçalves, M. d. C.; Nogueira, A. F. Preparação de nanopartículas de prata e ouro: um método simples para a introdução da nanociência em laboratório de ensino. *Química nova* **2012**, *35*, 1872−1878.
(35) Toma, H. E.; Bonifácio, L. d. S.; Anaissi, F. J. Da cor à cor inexistente: uma reflexão sobre espectros eletrônicos e efeitos cromáticos. *Quim. Nova* **2005**, *28* (5), 897−900.
(36) Lermusiaux, L.; Roach, L.; Lehtihet, M.; Plissonneau, M.; Bertry, L.; Buissette, V.; Le Mercier, T.; Duguet, E.; Drisko, G. L.; Leng, J.; et al. Silver nanoshells with optimized infrared optical response: synthesis for thin-shell formation, and optical/thermal properties after embedding in polymeric films. *Nanomaterials* **2023**, *13* (3), 614.
(37) Liu, X.; Ma, Z.; Xing, J.; Liu, H. Preparation and characterization of amino−silane modified superparamagnetic silica nanospheres. *J. Magn. Magn. Mater.* **2004**, *270* (1−2), 1−6.
(38) Ma, C. Y.; Dou, B. J.; Li, J. J.; Cheng, J.; Hu, Q.; Hao, Z. P.; Qiao, S. Z. Catalytic oxidation of benzyl alcohol on Au or Au−Pd nanoparticles confined in mesoporous silica. *Appl. Catal. B Environ.* **2009**, *92* (1−2), 202−208.
(39) Satyanarayana, M.; Goud, K. Y.; Reddy, K. K.; Gobi, K. V. Biopolymer stabilized nanogold particles on carbon nanotube support as sensing platform for electrochemical detection of 5-fluorouracil in-vitro. *Electrochim. Acta* **2015**, *178*, 608−616.
(40) Akolekar, D. B.; Bhargava, S. K. Investigations on gold nanoparticles in mesoporous and microporous materials. *J. Mol. Catal. A: Chem.* **2005**, *236* (1−2), 77−86.
(41) Veselinovic, J.; AlMashtoub, S.; Nagella, S.; Seker, E. Interplay of effective surface area, mass transport, and electrochemical features in nanoporous nucleic acid sensors. *Anal. Chem.* **2020**, *92* (15), 10751−10758.
(42) Preston, T. C.; Signorell, R. Growth and optical properties of gold nanoshells prior to the formation of a continuous metallic layer. *ACS Nano* **2009**, *3* (11), 3696−3706.
(43) Wang, J.; Schultze, J. W. Analytical electrochemistry. *Angew Chem. Int. Ed. Engl.* **1996**, *35* (17), 1998.
(44) Lee, S.-Y.; Lee, D.-J.; Yeon, K.-H.; Kim, W.-G.; Kang, M.-S.; Park, J.-S. A cyclic voltammetric study of electrodes for reverse electrodialysis. *J. Korean Electrochem. Soc.* **2013**, *16* (3), 145−150.
(45) Isotahdon, E.; Huttunen-Saarivirta, E.; Kuokkala, V.-T.; Paju, M. Corrosion behaviour of sintered Nd−Fe−B magnets. *Mater. Chem. Phys.* **2012**, *135* (2−3), 762−771.
(46) Fan, H.; Li, Y.; Wu, D.; Ma, H.; Mao, K.; Fan, D.; Du, B.; Li, H.; Wei, Q. Electrochemical bisphenol A sensor based on N-doped graphene sheets. *Anal. Chim. Acta* **2012**, *711*, 24−28.
(47) Ntsendwana, B.; Mamba, B.; Sampath, S.; Arotiba, O. Electrochemical Detection of Bisphenol A Using Graphene-Modified Glassy Carbon Electrode. *Int. J. Electrochem. Sci.* **2012**, *7* (4), 3501−3512.
(48) Shi, R.; Liang, J.; Zhao, Z.; Liu, A.; Tian, Y. An electrochemical bisphenol A sensor based on one step electrochemical reduction of cuprous oxide wrapped graphene oxide nanoparticles modified electrode. *Talanta* **2017**, *169*, 37−43.
(49) Su, B.; Shao, H.; Li, N.; Chen, X.; Cai, Z.; Chen, X. A sensitive bisphenol A voltammetric sensor relying on AuPd nanoparticles/graphene composites modified glassy carbon electrode. *Talanta* **2017**, *166*, 126−132.
(50) (a) Tu, X.; Yan, L.; Luo, X.; Luo, S.; Xie, Q. Electroanalysis of bisphenol A at a multiwalled carbon nanotubes-gold nanoparticles modified glassy carbon electrode. *Electroanalysis: An International Journal Devoted to Fundamental and Practical Aspects of Electroanalysis* **2009**, *21* (22), 2491−2494. (b) Zheng, Z.; Liu, J.; Wang, M.; Cao, J.; Li, L.; Wang, C.; Feng, N. Selective sensing of bisphenol A and bisphenol S on Pt/poly (diallyl dimethyl ammonium chloride)-diamond powder hybrid modified glassy carbon electrode. *J. Electrochem. Soc.* **2016**, *163* (6), B192−B199.
(51) Plowman, B. J.; Thompson, N.; O'Mullane, A. P. Probing the surface oxidation of chemically synthesised gold nanospheres and nanorods. *Gold Bull.* **2014**, *47*, 177−183.
(52) Wang, Y.; Laborda, E.; Crossley, A.; Compton, R. G. Surface oxidation of gold nanoparticles supported on a glassy carbon electrode in sulphuric acid medium: contrasts with the behaviour of 'macro'gold. *Phys. Chem. Chem. Phys.* **2013**, *15* (9), 3133−3136.
(53) Zhan, T.; Song, Y.; Tan, Z.; Hou, W. Electrochemical bisphenol A sensor based on exfoliated Ni2Al-layered double hydroxide nanosheets modified electrode. *Sens. Actuators, B* **2017**, *238*, 962−971.
(54) Santana, E. R.; de Lima, C. A.; Piovesan, J. V.; Spinelli, A. An original ferroferric oxide and gold nanoparticles-modified glassy carbon electrode for the determination of bisphenol A. *Sens. Actuators, B* **2017**, *240*, 487−496.
(55) Bhaskar, S.; Kowshik, N. C. S.; Chandran, S. P.; Ramamurthy, S. S. Femtomolar detection of spermidine using au decorated SiO2 nanohybrid on plasmon-coupled extended cavity nanointerface: a smartphone-based fluorescence dequenching approach. *Langmuir* **2020**, *36* (11), 2865−2876.
(56) Rai, A.; Bhaskar, S.; Ganesh, K. M.; Ramamurthy, S. S. Hottest hotspots from the coldest cold: welcome to Nano 4.0. *ACS Appl. Nano Mater.* **2022**, *5* (9), 12245−12264.
(57) Bhaskar, S.; Singh, A. K.; Das, P.; Jana, P.; Kanvah, S.; Bhaktha, B. N. S.; Ramamurthy, S. S. Superior resonant nanocavities engineering on the photonic crystal-coupled emission platform for

https://doi.org/10.1021/acsomega.3c03607
ACS Omega 2023, 8, 39023−39034

the detection of femtomolar iodide and zeptomolar cortisol. *ACS Appl. Mater. Interfaces* **2020**, *12* (30), 34323−34336.
(58) Bhaskar, S.; Thacharakkal, D.; Ramamurthy, S. S.; Subramaniam, C. Metal−dielectric interfacial engineering with mesoporous nano-carbon florets for 1000-fold fluorescence enhancements: smartphone-enabled visual detection of perindopril erbumine at a single-molecular level. *ACS Sustain. Chem. Eng.* **2023**, *11* (1), 78−91.

https://doi.org/10.1021/acsomega.3c03607
ACS Omega 2023, 8, 39023−39034